Geological noise removal in geophysical magnetic survey to detect unexploded ordnance based on image filtering

Maysam Abedi[1*], Kiomars Mosazadeh[2], Hamid Dehghani[3] and Ahmad MadanchiZare[2]

[1]*Assistant Professor, Department of Mining Engineering, College of Engineering, University of Tehran, Iran*
[2]*Instructor, Malek Ashtar University of Technology, Tehran, Iran*
[3]*Assistant Professor, Malek Ashtar University of Technology, Tehran, Iran*

(Received: 10 March 2014, accepted: 9 February 2015)

Abstract

This paper describes the application of three straightforward image-based filtering methods to remove the geological noise effect which masks unexploded ordnances (UXOs) magnetic signals in geophysical surveys. Three image filters comprising of mean, median and Wiener are used to enhance the location of probable UXOs when they are embedded in a dominant background geological noise. The study area consists of three buried UXOs while a geological dyke structure covers the magnetic anomaly of the desired objects. To provide a better representation of the actual locations of UXOs in the observed magnetic anomaly over this area, all image-based filters could appropriately separate the geological dyke effect from the UXOs. These image filters can be good candidates to remove the geological noise effect in UXO detection when encountering a mixed response of multi-source magnetic anomaly in contaminated territories with UXOs. An analytic signal map of the separated magnetic anomaly of UXOs was provided to enhance locations of the UXOs in the studied field. Also, a combination of the analytic signal and the Euler deconvolution methods were used to estimate the depth of three buried UXO targets in the study area indicating a high sensitivity of the estimated parameter to the noise level.

Keywords: Image filtering, geological noise removing, UXO detection, magnetic anomaly

1 Introduction

Shallow geophysical imaging methods are increasingly implemented in anomaly mapping of buried objects both on land and underwater. Geophysical explorations are vastly superior to the traditional surveys as they drastically minimize time, risk and cost factors (Pawlowski, 1994; Pawlowski et al., 1995). One of the main buried objects whose investigation is underway to develop appropriate geophysical approaches is the unexploded ordnances, called UXOs for brevity (Abedi et al., 2014).

The aim of the UXO cleanup over large contaminated territories is a sophisticated process in all military areas. In many

*Corresponding author: MaysamAbedi@ut.ac.ir

cases, the prospected UXOs are routinely detected by sensor sweeps (metal detectors) or geophysical surveys, relative to the background of the region of interest (geologic background and cultural clutter). Geophysical anomalies of UXO bodies result from the contrast in physical properties related to the host medium materials. Also, localized geological features and other buried cultural objects (comprising of noise objects in UXO detections such as ordnance scrap, cans, wire, etc.) yield physical property contrasts and subsequently cause undesirable geophysical anomalies (Figure 1). Since in many geological conditions, the physical property contrasts between a UXO and host medium are large, UXO detection is a straightforward process. The major problem in geophysical-based UXO detection is the existence of false alarms produced by noise objects, which needs discrimination algorithms in order to distinguish between varieties of anomaly sources. However, there is no general capability to effectively discriminate UXO geophysical anomalies from false alarm anomalies. It has been noted that for carefully executed geophysical surveys, the probability of UXO detection on documented test sites can exceed 90%. However, the false alarm rate of non-UXO targets excavated against each detected UXO remains quite high. Without discrimination capability between different causative sources, large numbers of false alarm anomalies must be considered as potential UXO sources, with approximately 75% of the cleanup cost spent on the project (Butler, 2000; Butler, 2003).

The widespread geophysical methods for UXO detections are total field magnetometers (TFM) and time domain electromagnetic induction (TDEM) (Bell et al., 2001; Beard et al., 2004; Pasion et al., 2007; Sanchez et al., 2008; Davis et al., 2010, 2011; Li et al., 2013). Application of these methods by experienced geophysical practitioners during demonstrations at controlled UXO test sites achieves probabilities of detection of UXO in excess of 90% (e.g. Pederson and Stalcup, 1997). Other geophysical methods which are worth less in a UXO detection consist of ground penetrating radar (GPR), frequency domain electromagnetic induction (FDEM) systems, multi-gate TDEM systems, multi-component TDEM systems, multi-component (vector) magnetometers, magnetic gradiometers, gravimetry, and their airborne systems (Bruschini et al., 1998; Huang and Won, 2000; Koppenjan et al., 2000; Butler, 2001; Butler et al., 2001; Butler, 2003; Huang and Won, 2003a, b, c; Huang and Won, 2004; Benavides and Everett, 2007; Billings and Youmans, 2007; Huang et al., 2007; Billings and Wright, 2010; Butler et al., 2012). The TFM and TDEM surveys from a helicopter platform at a 1-2 m sensor elevation have shown promise for covering large areas under UXO detection. Multi-gate (25–30 time gates), multi-component TDEM systems and multi-frequency FDEM systems are also of a valuable potential for UXO detection (Butler, 2000; Butler, 2003).

One of the main issues in UXO detection is the separation of UXO response from the background noise of the investigated area. The difficulty of separating background effect from UXO in contaminated terrain has been studied by Li et al. (2010) in a magnetic survey. They have developed a wavelet-based denoising algorithm and applied the iterative Wiener and high-pass Butterworth filters which appropriately removed the effect of the background geological noise in the UXO detection. In what follows, we are going to show that other image-based filtering techniques such as mean and median compared with Wiener method work well in such processes. These methods with straightforward implementations have been applied to a field study consisting of three buried UXOs embedded in a strong background geological noise arising from a dyke structure in a magnetic investigation. The analytic signal map of the UXO responses could also enhance those locations, but the estimated depths of these targets are highly sensitive to the level of the signal-to-noise ratio.

2 Methodology

The following sub-sections describe concisely three prevalent image-based filtering methods which were used in this study to separate UXO responses from geological noise. Moreover, the AN-EUL method is described to be applied in an in depth estimation of buried UXOs in the studied area.

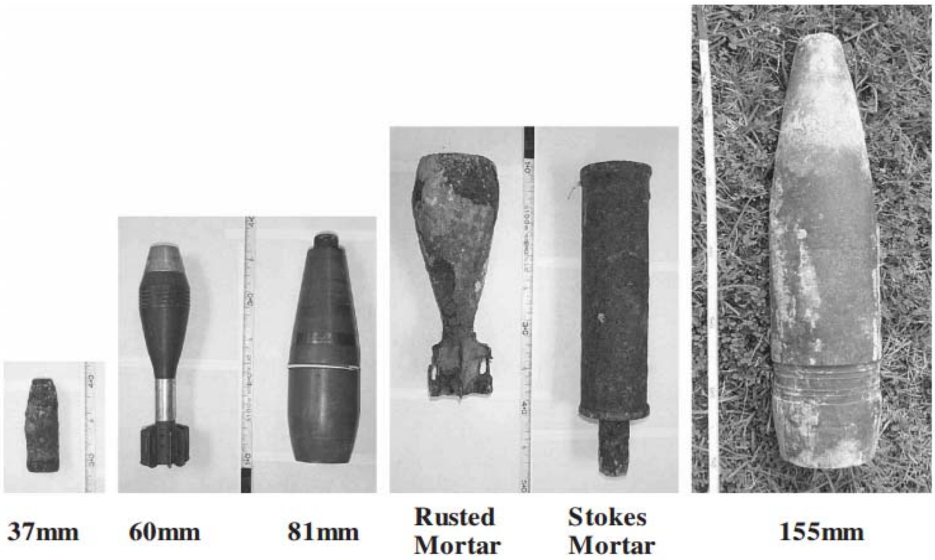

(a)

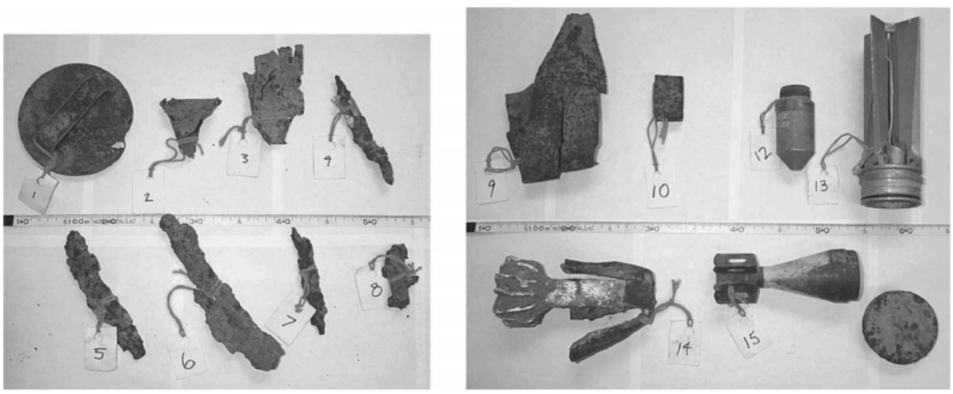

(b)

Figure 1. Some examples of buried objects in a UXO detection. (a) Some typical UXOs, (b) Some scrap targets (Pasion, 2007).

2.1 Mean Filter

The mean filter as an easy to implement the method of smoothing images is a sliding-window spatial filter that replaces the center value in the window with the average value of all the neighbouring pixels in the window which moves through all image pixels. The window can have any shape to smooth noisy images. The main problems associated with this filter are blurring of sharp edges in the image processing and dominating the average value of any pixel in its neighbourhood in the presence of high values of noise (impulsive noise). Therefore, the median filter has been widely used as it is very effective in removing such noise effect while preserving edges.

2.2 Median Filter

Median filtering is a nonlinear process useful in reducing impulsive, or salt-and-pepper noise. It is also useful in preserving edges in an image while reducing random noise. In a median filter, a window slides along the image, and the median intensity value of the pixels within the window becomes the output intensity of the pixel being processed (Lim, 1990).

2.3 Wiener Filter

Within the class of linear filters, the optimal filter for restoration in the presence of noise is given by the Wiener filter (Wiener, 1949). The filter assumes that the data is the sum of the signal and noise,

$$d(n,m) = s(n,m) + e(n,m), \qquad (1)$$

where d, s and e are the spatial representation of the data, signal and noise, respectively. In digital image processing, the 2D discrete image $d(n,m)$ is divided into N rows and M columns. The data value assigned to the integer coordinate (n,m) with $\{n = 1, 2, \ldots, N\}$ and $\{m = 1, 2, \ldots, M\}$ is $d(n,m)$. Here, we are looking for a signal estimator φ that simply scales the individual components of what is measured,

$$\hat{s}(n,m) = d(n,m)\varphi(n,m), \qquad (2)$$

where $\hat{s}(n,m)$ is the noise-free image and $\varphi(n,m)$ gives the optimal way of tapering off the noisy components, so as to give the best (L^2 norm) reconstruction of the original image. Therefore, $\varphi(n,m)$ minimizes the sum of squares of components, $\left\| \hat{s}(n,m) - s(n,m) \right\|_2^2$. Differentiating L^2 norm with respect to $\varphi(n,m)$ and setting it to zero gives $\bar{\varphi} = \left|\bar{s}\right|^2 \big/ \left|\bar{d}\right|^2$ in a Fourier domain. Here, $\bar{s}$ and $\bar{d}$ are the Fourier transform of the noise-free and the noise-corrupted images, respectively, and $\bar{\varphi}$ is the transfer function of a Wiener filter in a Fourier domain. To apply this filter to discrete image processing or spatial (pixel) basis implementation, the 2D Wiener filter for a sliding-window estimates the local mean (μ) and variance (σ^2) around each pixel as,

$$\mu = \frac{1}{nm} \sum_{n_1, m_1 \in D} d(n,m), \qquad (3)$$

and

$$\sigma^2 = \frac{1}{nm} \sum_{n_1, m_1 \in D} d^2(n,m) - \mu^2, \qquad (4)$$

where D is the n-by-m local neighborhood of each pixel in the image $d(n,m)$. Therefore, the Wiener filter estimates the center value in the window with the following equation,

$$w(n,m) = \mu + \varphi(n,m)\left[d(n,m) - \mu\right], \quad (5)$$

where $\varphi(n,m) = \left(\sigma^2 - \gamma^2\right)/\sigma^2$ and γ^2 is the noise variance. If the noise variance is not known in image processing, the mean of all the local estimated variances of sliding-window is used to calculate the Weiner output $w(n,m)$ (Lim, 1990; Khireddine et al., 2007; Press, 2008; Li et al., 2010).

2.4 The AN-EUL Method

To concisely describe formulation of the AN-EUL method, we need to explain briefly the analytic signal and the Euler method which are combined to generate simultaneously equations of the depth and the structural index (SI). The complex analytic signal can be defined as the horizontal and vertical derivatives of the potential data as follow (Nabighian, 1972, 1974, 1984),

$$A(x,y) = \left(\frac{\partial P}{\partial x}\hat{x} + \frac{\partial P}{\partial y}\hat{y} + i\,\frac{\partial P}{\partial z}\hat{z}\right), \quad (6)$$

where $\hat{x}$, $\hat{y}$ and $\hat{z}$ are unit vectors in the x, y and z directions, i is the imaginary number $\sqrt{-1}$, $\partial P/\partial z$; $\partial P/\partial x$ and $\partial P/\partial y$ are the vertical and horizontal derivatives of the potential data, respectively. The 3D calculation of the amplitude of the analytic signal (AAS) is,

$$\left|AAS(x,y)\right| = \sqrt{\left(\frac{\partial P}{\partial x}\right)^2 + \left(\frac{\partial P}{\partial y}\right)^2 + \left(\frac{\partial P}{\partial z}\right)^2}. \quad (7)$$

The amplitude of the nth-order derivative analytic signal is as follows,

$$\left|AAS_n(x,y)\right| = \sqrt{\left(\frac{\partial P_n^z}{\partial x}\right)^2 + \left(\frac{\partial P_n^z}{\partial y}\right)^2 + \left(\frac{\partial P_n^z}{\partial z}\right)^2}, \quad (8)$$

where the superscript z denotes the vertical derivative of potential data. The horizontal derivative can be simply calculated using the finite difference method or fast Fourier transform (FFT). The Hilbert transform in a frequency domain can be used to calculate the vertical derivative as well (Roest et al., 1992; Blakely, 1995; Debeglia and Corpel, 1997; Salem and Ravat, 2003; Davis et al., 2010).

Any 3D potential function $P(x,y,z)$ is said to be homogenous of degree n if the function obeys the following equation,

$$P(tx,ty,tz) = t^n P(x,y,z), \quad (9)$$

Then by differentiating Eq. (9) with respect to t, it can be shown that,

$$(x - x_0)\frac{\partial P}{\partial x} + (y - y_0)\frac{\partial P}{\partial y} + (z - z_0)\frac{\partial P}{\partial z} = N(B - P), \quad (10)$$

where (x_0, y_0, z_0) is the position of a potential source whose field is measured at (x,y,z). The potential field has a regional background value of B. Note that N (or SI) corresponds to $-n$ in Euler's Eq. (10) (Hood, 1965; Thompson, 1982; Blakely, 1995; Ravat, 1996; Salem and Ravat, 2003; Davis et al., 2010).

Taking the derivatives in the x, y and z directions of both Euler's Eq. (10) and also its first vertical derivative and setting $x = x_0$, $y = y_0$ and $z = 0$, we get the depth and the SI at the center of the source as follows,

$$z_0 = \left(\frac{|AAS_1||AAS_0|}{|AAS_2||AAS_0| - |AAS_1|^2} \right)_{x=x_0, y=y_0}, \quad (11)$$

$$N = \left(\frac{2|AAS_1|^2 - |AAS_2||AAS_0|}{|AAS_2||AAS_0| - |AAS_1|^2} \right)_{x=x_0, y=y_0}. \quad (12)$$

Equations (11) and (12) show that both the SI (which indicates the geometry of the source) and the depth of a potential anomaly can be simultaneously calculated from the *AAS* and its first- and second-order derivatives at the center of the potential source (Salem and Ravat, 2003).

3 Real Case Study

The study area, Chevallier Ranch area, is located approximately 10 miles north-northwest of Helena, Montana, USA. This area was selected because it contained a suite of geologic responses that have been identified as problematic for the magnetic surveying performed during the cleanup activities at Chevallier Ranch. Table 1 shows the depths and orientations of the buried ordnance objects. Total field magnetic data were collected at Chevalier Ranch in June, 2005. Figure 2 shows the residual magnetic anomaly over the study area indicating an extensive linear monopolar anomaly (>50 m strike length, ~100 nT) likely associated with a deeper mafic dyke (Li et al., 2010; Krahenbuhl et al., 2011). Three profiles from the residual magnetic data over UXOs have been shown in Figure 3 while dominated by the magnetic anomaly of the dyke structure. Three image-based filtering methods have been used to separate the response of UXOs from intense background anomaly arising from the dyke.

These filters comprising the mean, median and Wiener have been applied respectively to separate the magnetic anomaly of the multi-causative source in the study area. Figure 4 shows the outputs of the filtered image shown in Figure 2. Left column of Figure 4 indicates the magnetic anomaly from the dyke model

Table 1. UXOs locations and orientations buried at the study area.

ID	X (m)	Y (m)	Item	Inclination (degree)	Declination (degree)	Actual Depth (cm)	Estimated Depth (cm)
1	13	17	76 mm APT	0	0	11	6
2	20	20	76 mm TPT	0	90	9	5
3	27	23	76 mm APT	8 (nose up)	82	9	3

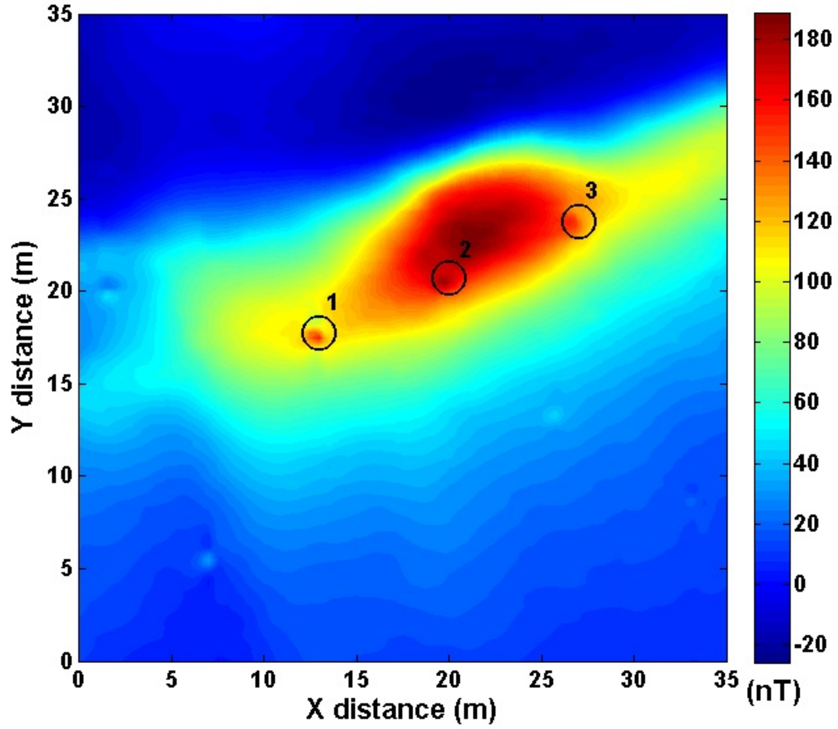

Figure 2. The residual magnetic anomaly over the study area. The locations of the buried UXOs have been superimposed on the observed data with dark circles.

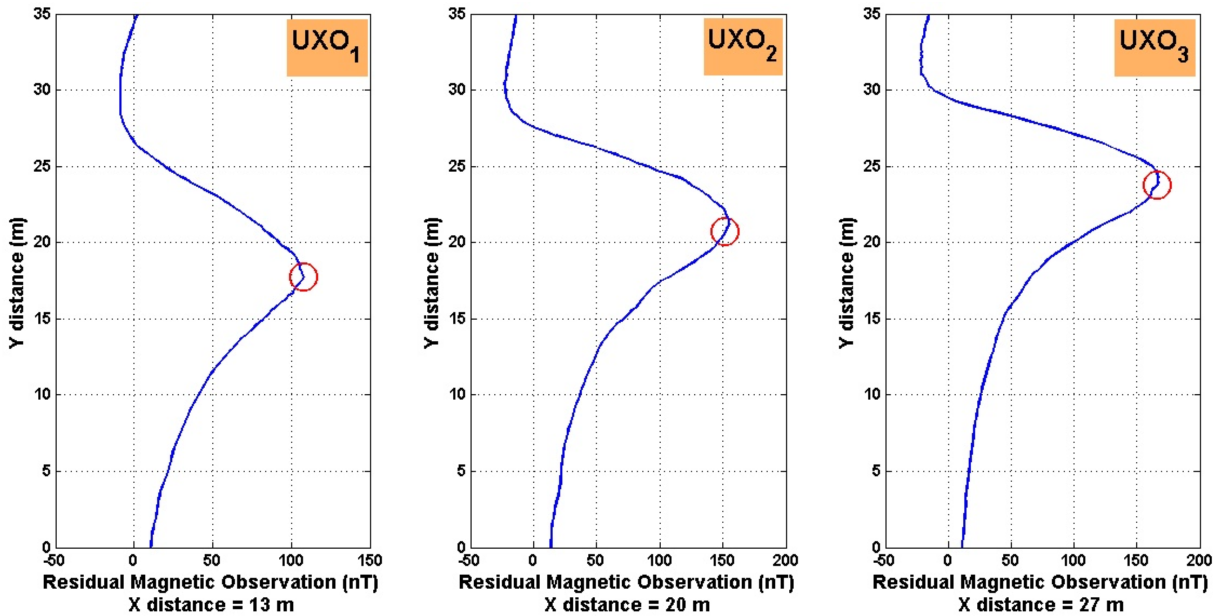

Figure 3. Residual magnetic observation along three profiles over the buried UXOs. The locations of UXOs have been superimposed on the observed data with red circles.

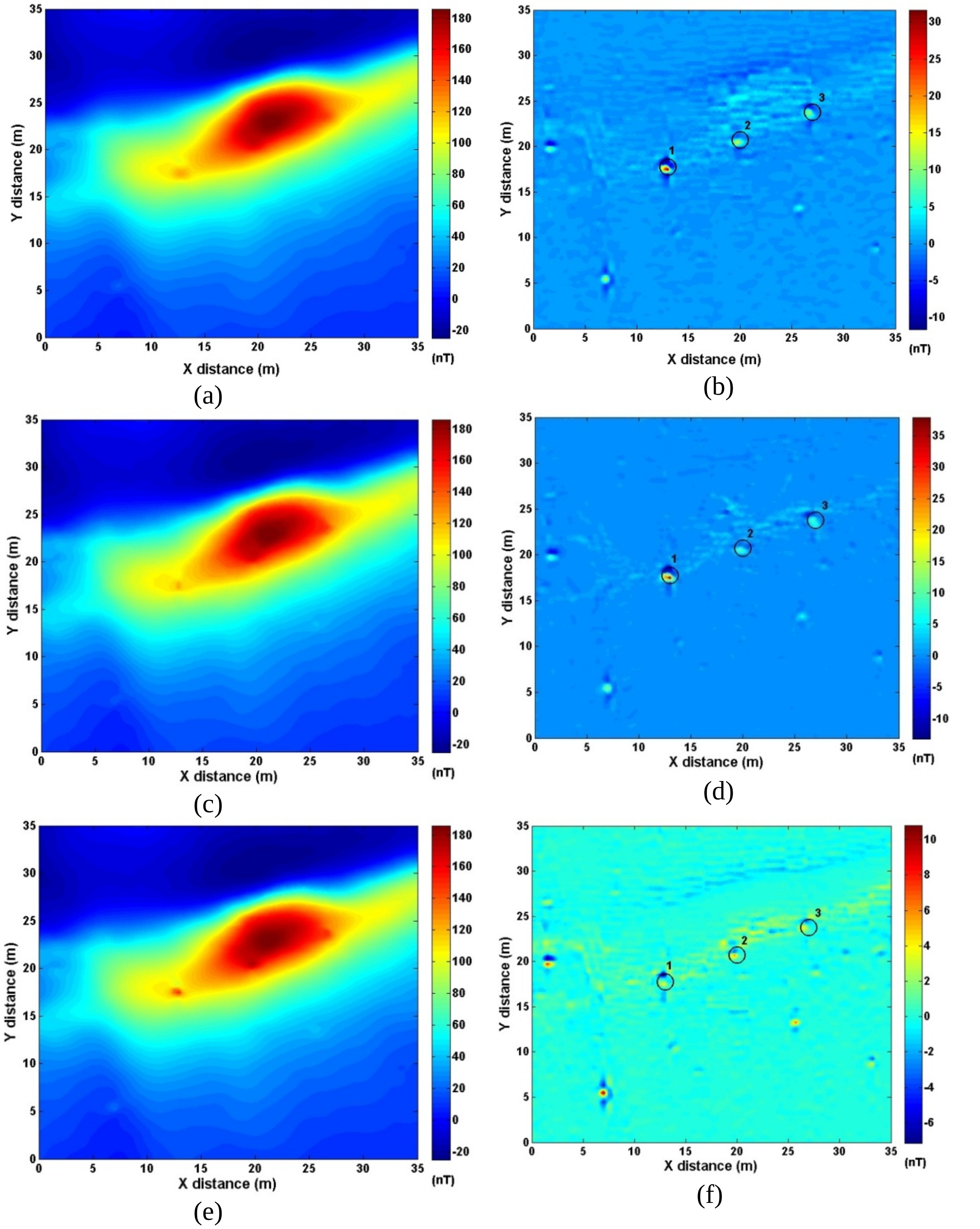

Figure 4. Image-based filtering methods for multi-source magnetic anomaly separation. The left column shows the geological noise effect of the dyke structure, and the right one is the UXOs response anomaly. Figures 4a and 4b are derived from the mean filter: 4c and 4d are from the median filter, and 4e and 4f are from the Wiener filter assuming a 5×5-pixel sliding-window. The locations of the buried UXOs have been superimposed on the right column with dark circles.

which has a geological noise effect in the UXO cleanup process in the contaminated territories. The right column shows the UXO response acquired from three methods, i.e. mean, median and Wiener, respectively. Aforementioned filters show that the mean filter is sensitive to impulsive noise and the Wiener worked well when the variance of the noise was known. All methods could separate the magnetic response of three buried UXOs while the median filter was less sensitive to the noise effect. Here, we assumed a sliding-window of 5×5-pixel. The analytic signal maps of the UXO response were also provided in order to enhance the locations of buried objects in Figure 5. Here, the analytic signal map, as applied by Nabighian (1972, 1974 and 1984), could enhance those locations based on the directional derivatives of the UXO's magnetic anomaly.

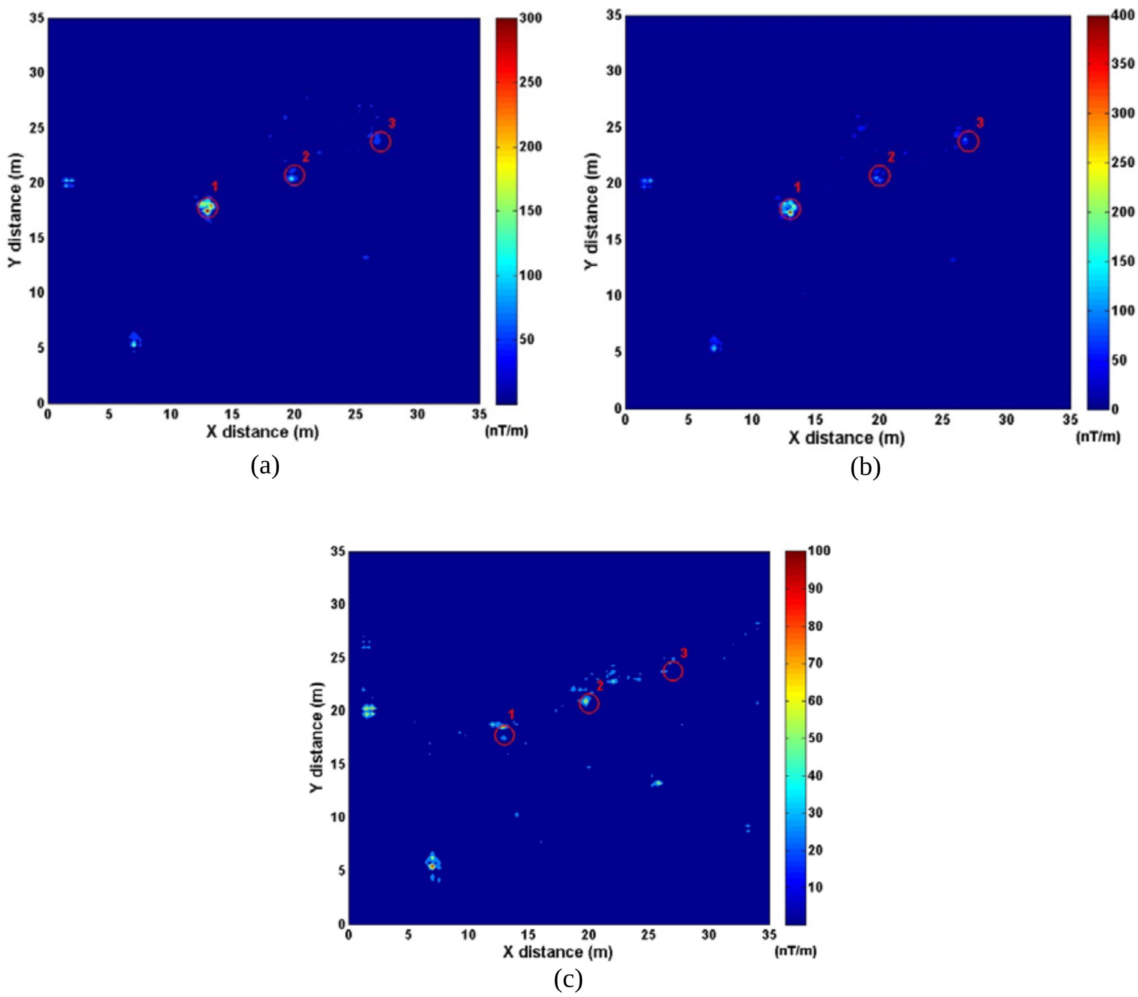

Figure 5. The analytic signal method for enhancing the locations of UXO targets. The analytic signal maps are applied to the UXO response acquired from (a) the mean filter, (b) the median and (c) the Wiener filter. The actual locations of the buried UXOs have been superimposed on the observed data with red circles.

4 Discussion

All filtered maps in the right column of Figure 4 could appropriately detect the actual locations of UXOs in the study area but the point should be noted is the detection of some scraps in addition to UXOs. These false alarms that are not associated with a UXO could drastically increase the cost of conducted projects in UXO cleanup stage to excavate false alarms arising from scrap targets. Figure 6 shows the probable locations of the desired targets while four out of seven are related to the scraps.

Here, we have estimated the depth of the buried UXO objects using the automatic method, i.e. AN-EUL approach. Table 1 shows the estimated depth of UXOs which are located at near surface. Since the magnetic signals of these objects were weak and also sensitive to the noise level of the study area, those depths were a bit different from the actual ones in Table 1. Therefore, the low signal-to-noise ratio of magnetic response of UXO could affect the estimated depth of the buried objects when locating in a high level of background noise.

5 Conclusions

This paper described the application of three image-based filtering methods comprising the mean, median and Wiener filters. These methods could appropriately separate the magnetic response of some buried UXO targets from the background geological noise arising from a dyke structure. The analytic signal map of the filtered magnetic response also enhanced the locations of UXO targets in the study area. The estimated depth of the buried UXO using a combination of the analytic signal and the Euler deconvolution methods (AN-EUL) had a bit lack of accuracy because of the low magnetic intensity of the UXO response with regard to a high level of noise.

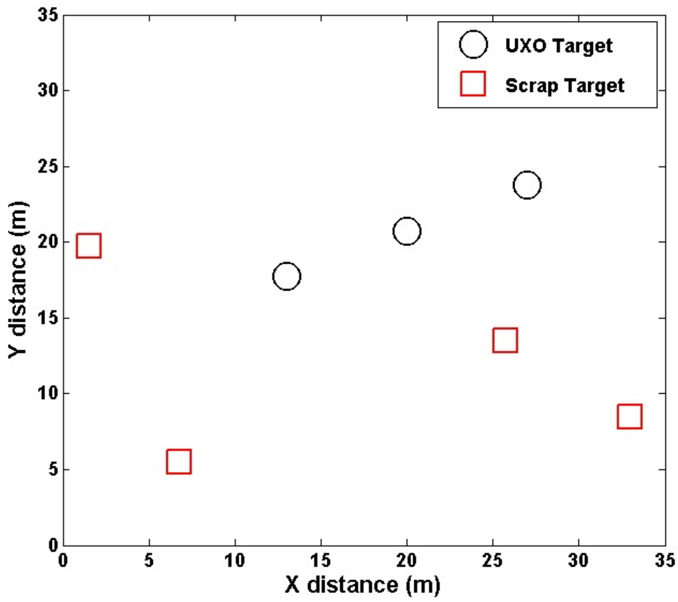

Figure 6. UXO detection based on the image filtering outputs shown in Figure 4.

Acknowledgements

The authors gratefully acknowledge the elite foundation office at the Malek Ashtar University of Technology, Tehran. We thank the College of Mining Engineering at the University of Tehran allowing the first author to do this project besides the PhD thesis. We also thank Prof. Misac Nabighian from Center for Gravity, Electrical, & Magnetic Studies, Department of Geophysics at Colorado School of Mines for providing data.

References

Abedi, M., Mosazadeh, K., Dehghani, H., and MadanchiZare, A., 2014, Enhancing magnetic signals in unexploded ordnances (UXO) detection based on edge-preserved stable downward continuation method: Journal of Mining & Environment, **5**, 13-24.

Beard, L. P., Doll, W. E., Holladay, J. S., Gamey, T. J., Lee, J. L. C., and Bell, D. T., 2004, Field tests of an experimental helicopter time-domain electromagnetic system for unexploded ordnance detection: Geophysics, **69**, 664-673.

Bell, T., Barrow, B., Miller, J., and Keiswetter, D., 2001, Time and frequency domain electromagnetic induction signatures of unexploded ordnance: Subsurface Sensing Technology and Applications, **2**, 153-175.

Benavides, A., and Everett, M. E., 2007, Non-linear inversion of controlled source multi-receiver electromagnetic induction data for unexploded ordnance using a continuation method: J. Appl. Geophys., **61**, 243-253.

Billings, S. D., and Youmans, C., 2007, Experiences with unexploded ordnance discrimination using magnetometry at a live-site in Montana: J. Appl. Geophys., **61**, 194-205.

Billings, S. D., and Wright, D., 2010, Interpretation of high-resolution low-altitude helicopter magnetometer surveys over sites contaminated with unexploded ordnance: J. Appl. Geophys., **72**, 225-231.

Blakely, R. J., 1995, Potential Theory in Gravity and Magnetic Applications: Cambridge University Press.

Bruschini, C., Gros, B., Guerne, F., Piéce, P. Y., and Carmona, O., 1998, Ground penetrating radar and imaging metal detector for antipersonnel mine detection: J. Appl. Geophys., **40**, 59-71.

Butler, D. K., 2000, Assessment of Microgravity for UXO Detection and Discrimination: U.S. Army Engineer Research and Development Center, 1-37.

Butler, D. K., 2001, Potential fields methods for location of unexploded ordnance: The Leading Edge, **20**, 890–895.

Butler, D. K., Wolfe, P. J., and Hansen, R. O., 2001, Analytical modeling of magnetic and gravity signatures of unexploded ordnance: J. Environmental and Engineering Geophysics, **6**, 33 – 46.

Butler, D. K., 2003, Implications of magnetic backgrounds for unexploded ordnance detection: J. Appl. Geophys., **54**, 111-125.

Butler, D. K., Simms, J. E., Furey, J. S., and Bennett, H. H., 2012, Review of magnetic modeling for UXO and applications to small items and close distances: J. Environmental and Engineering Geophysics, **17**, 53-73.

Davis, K., Li, Y., and Nabighian, M. N., 2010, Automatic detection of UXO magnetic anomalies using extended

Euler deconvolution: Geophysics, **75**, G13-G20.

Davis, K., Li, Y., and Nabighian, M. N., 2011, Effects of low-pass filtering on the calculated structure index from magnetic data: Geophysics, **76**, L23-L28.

Debeglia, N., and Corpel, J., 1997, Automatic 3-D interpretation of potential field data using analytic signal derivatives: Geophysics, **62**, 87-96.

Hood, P., 1965, Gradient measurements in aeromagnetic surveying: Geophysics, **30**, 891-902.

Huang, H., and Won, I. J., 2000, Conductivity and susceptibility mapping using broadband electromagnetic sensors: J. Environmental and Engineering Geophysics, **5**, 31-41.

Huang, H., and Won, I. J., 2003a, Detecting metal objects in magnetic environments using a broadband electromagnetic method: Geophysics, **68**, 1877-1887.

Huang, H., and Won, I. J., 2003b, Automatic anomaly picking from broadband electromagnetic data in an unexploded ordnance (UXO) survey: Geophysics, **68**, 1870-1876.

Huang, H., and Won, I. J., 2003c, Characterization of UXO-like targets using broadband electromagnetic induction sensors: IEEE Trans. Geosci. Remote Sensing, **41**, 652-663.

Huang, H., and Won, I. J., 2004, Electromagnetic detection of buried metallic objects using quad-quad conductivity: Geophysics, **69**, 1387-1393.

Huang, H., SanFilipo, B., Oren, A., and Won, I. J., 2007, Coaxial coil towed EMI sensor array for UXO detection and characterization: J. Appl. Geophys., **61**, 217-226.

Khireddine, A., Benmahammed, K., and Puech, W., 2007, Digital image restoration by Wiener filter in 2D case: Advances in Engineering Software, **38**, 513-516.

Koppenjan, S. K., Allen, C. M., Gardner, D., Wong, H. R., Lee, H., and Lockwood, S. J., 2000, Multi-frequency synthetic-aperture imaging with a lightweight ground penetrating radar system: J. Appl. Geophys., **43**, 251-258.

Krahenbuhl, R., Li, Y., Nabighian, M., Davis, K., and Billings, S., 2011, Advanced UXO Detection and Discrimination Using Magnetic Data Based on Extended Euler Deconvolution and Shape Identification through Multipole Moments: SERDP Project MR-1638, p. 117.

Li, Y., Krahenbuhl, R., Meglich, T., Oldenburg, D., Pasion, L., Billings, S., Van Dam, R., and Harrison, B., 2010, Improving UXO Detection and Discrimination in Magnetic Environments: SERDP Project MM-1414, p. 278.

Li, Y., Devriese, S. G. R., Krahenbuhl, R., and Davis, K., 2013, Enhancement of magnetic data by stable downward continuation for UXO application: IEEE Trans. Geosci. Remote Sensing, **51**, 3605-3614.

Lim, Jae S., 1990, Two-Dimensional Signal and Image Processing: Englewood Cliffs, NJ, Prentice Hall, p. 548.

Nabighian, M. N., 1972, The analytic signal of two-dimensional magnetic bodies with polygonal cross-section: its properties and use for automated anomaly interpretation: Geophysics, **37**, 507–517.

Nabighian, M. N., 1974, Additional comments on the analytic signal of two dimensional magnetic bodies with polygonal cross-section: Geophysics, **39**, 85–92.

Nabighian, M. N., 1984, Toward a three-dimensional automatic interpretation of potential field data via generalized Hilbert transforms: Fundamental relations: Geophysics, **49**, 780–786.

Pasion, L. R., 2007, Inversion of time domain electromagnetic data for the detection of unexploded ordnance: PhD Thesis, The University of British Columbia.

Pasion, L. R., Billings, S. D., Oldenburg, D. W., and Walker, S. E., 2007, Application of a library based method to time domain electromagnetic data for the identification of unexploded ordnance: J. Appl. Geophys., **61**, 279-291.

Pawlowski, J., 1994, Ordnance Investigation Using an Electromagnetic Method, Lake Erie, Port Clinton, Ohio: report for USAE Waterways Experiment Station, by Geophysics Ltd., Mississauga, Ontario.

Pawlowski, J., Lewis, R., Dobush, T., and Valleau, N., 1995, Proceeding of the Symposium on the Application of Geophysics to Engineering and Environmental Problems, Orlando, Florida, USA.

Pederson, A., and Stalcup, B., 1997, Phase III advanced technology demonstrations at Jefferson proving ground: Proceedings of the UXO Forum' 97: pp. 281 – 289.

Press, W. H., 2008, Computational Statistics with Application to Bioinformatics: Unit 19, Wiener Filtering (and some Wavelets), The University of Texas at Austin.

Ravat, D., 1996, Analysis of the Euler method and its applicability in environmental magnetic investigations: J. Environmental and Engineering Geophysics, **1**, 229-238.

Roest, W. R., Verhoef, J., and Pilkington, M., 1992, Magnetic interpretation using 3-D analytic signal: Geophysics, **57**, 116-125.

Salem, A., and Ravat, D., 2003, A combined analytic signal and Euler method (AN-EUL) for automatic interpretation of magnetic data: Geophysics, **68**, 1952-1961.

Sanchez, V., Li, Y., Nabighian, M. N., and Wright, D. L., 2008, Numerical modeling of higher order magnetic moments in UXO discrimination: IEEE Trans. Geosci. Remote Sensing, **46**, 2568-2583.

Thompson, D. T., 1982, "EULDPH" A new technique for making computer-assisted depth estimates from magnetic data: Geophysics, **47**, 31-37.

Wiener, N., 1949, Extrapolation, interpolation, and smoothing of stationary time series: Cambridge, MIT.